Abstract

Lithium-metal anodes coupled with high-nickel ternary cathodes offer the potential for high-energy-density batteries. However, the practical cycling stability of lithium-metal batteries poses a significant challenge due to the hydrolysis reaction of $LiPF_6$ in common commercial electrolytes and the unstable electrode-electrolyte interface at high temperatures. Here we demonstrate that stable cycling can be realized by using an appropriate amount of multifunctional sacrificial additives, triethoxy(3,3,3-trifluoropropyl)silane (TTFS). The cycling stability is ascribed to the TTFS's ability to inhibit the hydrolysis of $LiPF_6$ by the presence of strong Si−O bond, which efficiently captures trace H_2O and HF in common electrolytes. In addition, TTFS contributes to preferentially form robust interfaces on both anodes and cathodes, leading to the inhibition of capacity degradation in the cell. The $Li||LiNi_{0.8}Co_{0.1}Mn_{0.1}O_2$ cell retains a capacity retention rate of 62.1% after 500 cycles at 25℃ and 81.2% after 160 cycles at a high temperature 60℃, advancing practical lithium-metal batteries.

Keyword: Lithium metals; Sacrificial additives; Electrode-electrolyte interphases; Water hazards

Introduction

Lithium-metal batteries (LMBs) have emerged as a promising technology due to the high specific capacity (3860 mAh g^{-1}) and low reduction potential (−3.04 V vs. the standard hydrogen electrode) of Li metal anode.[1–6] However, the high reactivity between the electrolyte and Li metal results in a low Coulombic efficiency (CE) in LMBs, leading to issues such as Li dendrite growth that seriously impact the cycling performance of these batteries.[7–11] The growth of Li dendrites can breach the diaphragm (e.g., polyethylene, polypropylene), causing a short circuit within the battery and potentially giving rise to safety hazards.[12–17] This risk is heightened when utilizing high-voltage nickel-rich cathodes such as $LiNi_{0.8}Co_{0.1}Mn_{0.1}O_2$ (NCM811).[18–21] The selection of an appropriate electrolyte plays a critical role in maintaining the stability of the cathode material, particularly in matching the requirements of high-voltage cathodes. Although the commonly used organic electrolyte containing $LiPF_6$ and carbonate is prevalent, it has drawbacks as the decomposition of $LiPF_6$ yields PF_5, leading to the generation of HF upon interaction with residual water in the electrolyte. Subsequently, the HF can corrode the high-nickel cathodes, resulting in the excessive dissolution of transition metals (TMs), ultimately diminishing the battery capacity and fostering undesirable occurrences like cathode gas generation.[22–26] In environments characterized by elevated temperatures, the hydrolysis reaction of $LiPF_6$ intensifies, exacerbating the reactivity between the electrolyte and the electrode.

Numerous research efforts have been dedicated to addressing the challenges associated with electrolyte stability in LMBs. Various strategies have been explored, including the utilization of more stable electrolyte solvents,[27–31] introduction of beneficial additives into the electrolyte,[32–34] and the development of artificial solid-electrolyte interphase (SEI).[35–39] Among these approaches, the addition of additives to the electrolyte stands out as a straightforward and effective method for enhancing electrolyte stability and safeguarding the electrodes simultaneously. A range of functional additives,

such as organosilicones (e.g., silanes, silazanes, siloxanes),[40–42] organofluorines (e.g., fluorocarbons),[43,44] organophosphates (e.g., phosphates),[45,46] and organonitriles (e.g., nitrile, amine groups),[47] have displayed positive effects on the electrolyte interface. These additives have demonstrated the ability to improve the stability between the electrolyte and electrodes, thus enhancing the cycling stability of LMBs. Notably, siloxane compounds containing Si−O bonds have proven effective in inhibiting the hydrolysis reaction of $LiPF_6$ and trapping HF generated during hydrolysis.[48] Research by Liu et al. highlighted the incorporation of propargyloxytrimethylsilane into the electrolyte as an effective method for capturing corrosive HF, thereby inhibiting the dissolution of transition metals.[49] Additionally, Ma et al. discovered that the inclusion of bisfluoroacetamide as an additive led to the formation of a stable interfacial phase at the anode, attributed to the introduction of C−F bonds.[50] However, current findings suggest that most additives tend to form cathode-electrolyte interphase (CEI) and SEI exclusively at one electrode. Therefore, there is an urgent need for suitable multifunctional electrolyte additives, which can inhibit the hydrolysis of $LiPF_6$ as well as simultaneously form robust interfaces on both electrodes.

In this study, we demonstrate a multifunctional sacrificial additive, triethoxy(3,3,3-trifluoropropyl)silane (TTFS), enables stable cycling performance in practical LMBs, particularly in high-temperature environments (**Figure 1**). The effectiveness of TTFS is demonstrated through its ability to capture trace H_2O in the electrolyte and neutralize corrosive HF that results from the hydrolysis of $LiPF_6$. Furthermore, TTFS alters the solvent structure surrounding Li^+, thereby reducing the likelihood of solvent decomposition at the electrode interface. Notably, TTFS has a higher highest occupied molecular orbital (HOMO) and a lower lowest unoccupied molecular orbital (LUMO), facilitating the formation of robust SEI and CEI at both anode and cathode, respectively. The incorporation of TTFS leads to enhanced cycling performance of LMBs, as evidenced by Li||Li cells

exhibiting stable cycling for 500 hours at 1 mA cm^{-2}. Moreover, Li||NCM811 cells showcase a capacity retention rate of 62.1% after 500 cycles at 1 C at 25°C. Even with a temperature increase to 60°C, the Li||NCM811 cell retains a capacity retention rate of 62.1% after 160 cycles. This research offers an effective solution by introducing multifunctional electrolyte additives to extend the cycling life of LMBs.

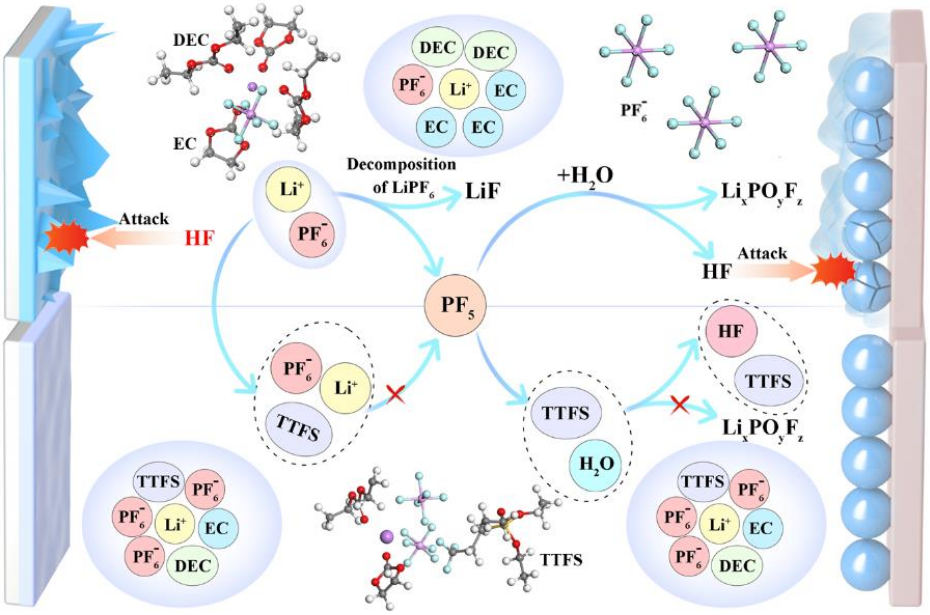

Figure 1. Schematic diagram of hydrolysis reaction of $LiPF_6$ and mechanism of TTFS.

Results and discussion

To investigate the impact of TTFS on the composition and structure of the SEI, molecular dynamics (MD) simulations and density-functional theory (DFT) theoretical calculations were first carried out to analyze alterations in the solvation structure of Li^+ following the addition of TTFS. The findings displayed in **Figure 2**a and b revealed significant changes. Upon introducing TTFS, the coordination numbers of EC and DEC decreased from 2.33 to 1.70 and 0.80 to 0.69, respectively, indicating reduced solvent decomposition likelihood at the electrode. Furthermore, the coordination number of PF_6^- increased from 1.35 to 1.85, demonstrating enhanced involvement of PF_6^- in the solvation structure, which facilitates the formation of an anion-derived electrode/electrolyte interface on the electrode surface. In Figure 2c, the electron surface potential (ESP) charge and electron density distributions of

TTFS are depicted. Notably, TTFS exhibits a substantial dipole moment of 3.04 D, implying a high likelihood of coordination with Li^+.[22] This conjecture is substantiated in Figure S1 as well as in Figures 2e and 2f. The MD simulations reveal that, in the solvated structure of the first Li^+ layer, the introduction of TTFS leads to its active participation in Li^+ coordination in this layer. Consequently, a significant decline in solvent-ligand coordination with Li^+ is observed alongside an augmentation in PF_6^- coordination following the inclusion of TTFS. Subsequently, the HOMO and LUMO of TTFS with EC, DEC, and $LiPF_6$ were determined. In Figure 2d, it is clear that TTFS has the lowest LUMO and the highest HOMO compared to the other solvents, suggesting that TTFS has preferential oxygen reduction at the electrode, favoring the formation of SEI and CEI. The linear scan voltage (LSV) curves for cells utilizing different electrolytes are depicted in Figure 2g and S2. Notably, the oxidation curve of TTFS-BE illustrates a distinctive peak at around 4.2 V, signifying the additive's ability to preferentially passivate the cathode of NCM811. In addition, TTFS initiates reduction at 2.4 V, whereas BE undergoes reduction at 1.9 V. This means that TTFS can be preferentially reduced on lithium metal anodes, thereby protecting other solvents. Additionally, through DFT calculations, the adsorption energies of the additive molecules and each solvent on the cathode surface of NCM811 were evaluated (Figure 2h). TTFS exhibited the lowest adsorption energy (−4.97 eV) compared to PF_6^- (−2.70 eV), EC (−1.77 eV), and DEC (−3.51 eV), indicating TTFS's rapid participation in the formation of the CEI for faster passivation than other solvents. Subsequent X-ray photoelectron spectroscopy (XPS) analysis of the NCM811 cathode surface before and after TTFS-BE infiltration confirmed the presence of characteristic peak signals of TTFS post-infiltration (Figure 2i), aligning with theoretical predictions and verifying TTFS's preferential oxidation on the cathode surface.

A series of experiments were conducted to provide a detailed description of TTFS's ability to eliminate water hazards. Nuclear magnetic resonance (NMR) tests were performed after 1000 ppm

water was added to BE and TTFS-BE for 12 hours, and ^{19}F NMR spectra was shown in Figure 2j and k. In the BE electrolyte, distinct peaks at around 168 ppm and 78 ppm were visible, deriving from $LiPF_6$ hydrolysis products of $PO_2F_2^-$ and HF, respectively, indicating a reaction with trace amounts of H_2O. However, after the addition of TTFS, these characteristic peaks of $LiPF_6$ hydrolysis products were no longer detected, showcasing TTFS's significant inhibition of $LiPF_6$ hydrolysis. This inhibition can be attributed to the presence of strong Si−O bonds in TTFS, spontaneously capturing HF and trace H_2O in the electrolyte. Consequently, it can be inferred that TTFS effectively prevents $LiPF_6$ hydrolysis. Moreover, the binding energy (ΔE) between TTFS and water, as well as between TTFS and HF, was assessed through DFT theoretical calculations. The results displayed in Figure 2l and S3 revealed that the ΔE of TTFS with H_2O was −27.73 kJ mol^{-1}, significantly higher than that of $LiPF_6$ with H_2O (−19.25 kJ mol^{-1}), aligning with the NMR findings and highlighting TTFS's water adsorption capacity. Furthermore, the ΔE between TTFS and HF was calculated to be −37.98 kJ mol^{-1}, supporting TTFS's spontaneous adsorption of HF. In conclusion, the combined outcomes of experiments and theoretical calculations affirm TTFS's efficacy in mitigating water hazards by impeding the hydrolysis of $LiPF_6$.

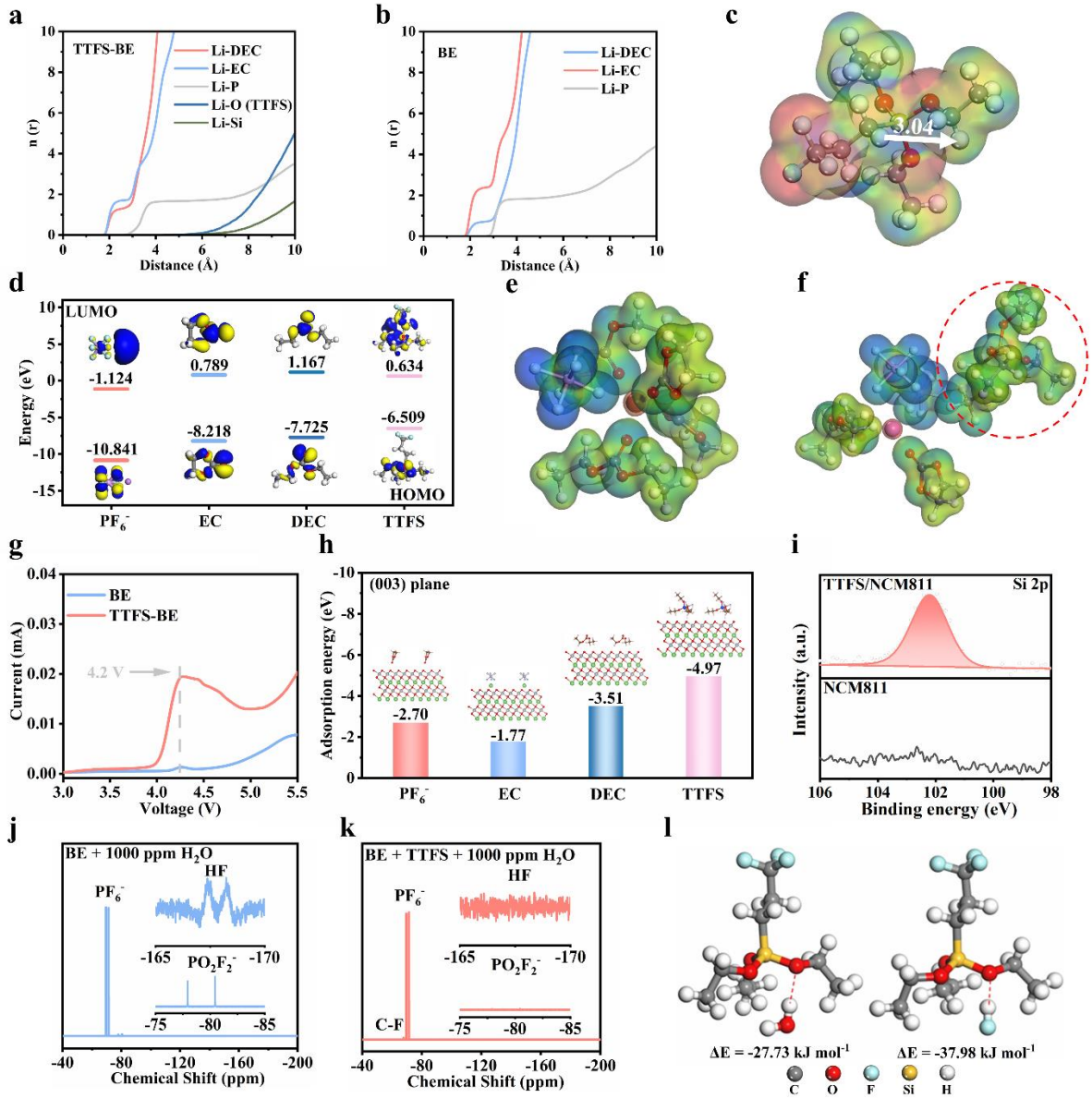

Figure 2. Coordination number of Li^+ in (a) BE and (b) TTFS-contained electrolyte systems. (c)The ESP charges and electron density distribution as well as the dipole moment of the HFAC molecule. (d) LUMO and HOMO energy of $LiPF_6$, EC, DEC, and TTFS. The simulated first solvation structures of Li^+ in (f) BE and (i) TTFS-contained electrolytes. (g) LSV curves for BE and TTFS-BE at scan rate of 0.5 mV s^{-1}. (h) Adsorption energy of TTFS, PF_6^-, EC, and DEC on (003) plane of NCM811 cathode. (i) Si 2p XPS spectra of pristine NCM811 cathode and electrolyte (TTFS-added) immersed NCM811 cathode. ^{19}F NMR spectra of 1000 ppm H_2O containing electrolyte after 6 h storage, j) without additive and (k) with TTFS additive. (l) Binding energies of H_2O-TTFS and HF-TTFS.

To assess the effectiveness of TTFS, the impact of TTFS on the high voltage cathode was investigated. Li||NCM811 cells were constructed using a base electrolyte (BE) and a base electrolyte with 0.5 wt% TTFS added (TTFS-BE). The Li||NCM811 cell with TTFS-BE demonstrated notable enhancements, as evidenced by a capacity retention of 62.1% and an average CE of 99.69% after 500

cycles at room temperature at a rate of 1 C, as depicted in **Figure 3**a and S4. In contrast, the Li||NCM811 cell assembled with BE exhibited a mere 37.6% capacity retention and a reduced average CE of 97.9% under identical conditions. It is evident that the cycling stability of TTFS-BE is significantly better than that of BE and other recently reported additives (Table S1). It should be emphasized that we also assembled Li||NCM811 cells with a highly loaded cathode (21.5 mg cm^{-2}). As shown in Figure S5, the cell using TTFS-BE as the electrolyte achieved stable cycling with 85.4% capacity retention after 100 cycles. This result contrasts with the battery using BE as the electrolyte, which exhibited significant rapid capacity decay, further highlighting the potential of TTFS in practical applications.

Moreover, the incorporation of TTFS ameliorated the rate performance of Li||NCM811 cells, substantiated by Figure 3b, and the cyclic voltammetry (CV) curves of Li||NCM811 cells assembled with distinct electrolytes, indicating the positive influence of TTFS (Figure 3c and S6). An additional oxidation peak emerged at 4.2 V, indicative of TTFS participation in the formation of CEI. Post the initial cycle, the oxidation peak at 3.9 V transitioned to 3.75 V and remained steady in subsequent cycles, implying that TTFS addition conferred increased stability to the NCM811 cathode. Notably, the efficacy of TTFS in enhancing the cycle life of Li||NCM811 cells was more pronounced at a higher temperature of 60°C, where $LiPF_6$ hydrolysis is exacerbated. At this elevated temperature and a 1 C rate, the Li||NCM811 cell fabricated with BE electrolyte retained only 54.1% of its initial capacity after 160 cycles (Figure 3d and e), primarily due to the heightened hydrolysis of $LiPF_6$ leading to expedited capacity decay. Conversely, the cell assembled with TTFS-BE electrolyte retained 81.2% capacity after 160 cycles under the same conditions. Furthermore, the introduction of TTFS additive improved the rate performance of the Li||NCM811 cell even at elevated temperatures up to 60°C, as depicted in Figure 3f. To ascertain the stability of TTFS in extreme conditions, BE and TTFS-BE were left exposed to air at 50% relative humidity (RH) for 12 h, without encapsulation or a nitrogen atmosphere control (Figure

3g). Subsequently, Li||NCM811 cells were constructed using these two electrolytes individually. Results illustrated that the cell with TTFS-BE exhibited typical charge/discharge behavior (Figure 3h). Conversely, the cell assembled with BE exposed to air at 50% RH displayed significant fluctuations in the charging curve and completely lost its discharging ability. After disassembling the battery, it was observed that the lithium metal anode using BE exhibited severe corrosion, which was identified as the primary reason for the battery failure (Figure S7). Conversely, the battery utilizing TTFS-BE displayed almost no corrosion, indicating sustained stability in battery operation. This underscores the effectiveness of TTFS in alleviating water-related risks even under harsh conditions, consequently prolonging the cycle life of the LMBs. In summary, the capacity of TTFS to mitigate water-related hazards in extreme environments serves to enhance the longevity of the LMBs.

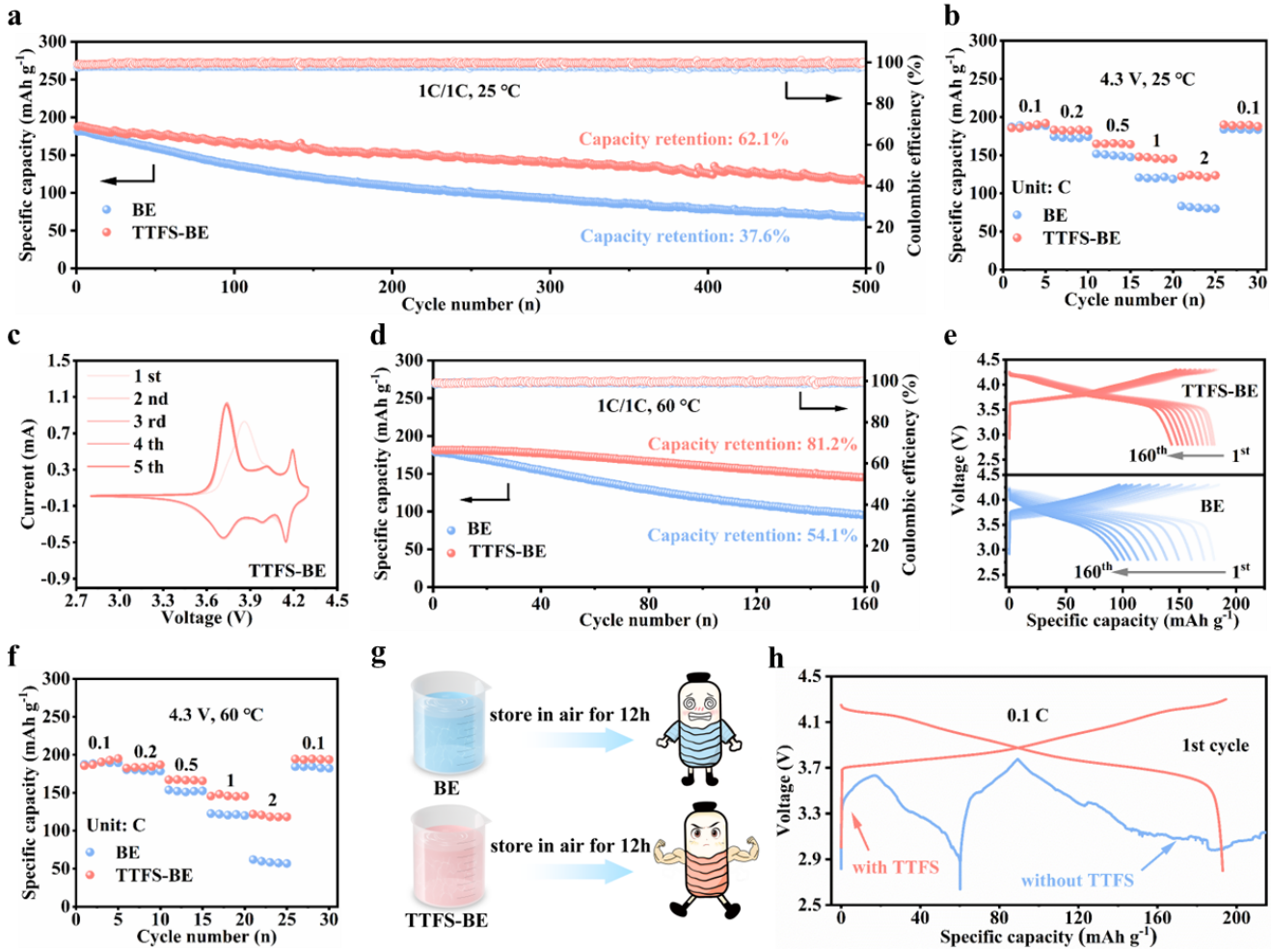

Figure 3. (a) Cycling performance and (b) rate capability of Li||NCM811 cells in BE and TTFS-BE. (c)

CV curves of the Li||NCM811 cell with TTFS contained electrolyte with a scan rate of 0.1 mV s^{-1}. (d) Cycling performance of Li||NCM811 cells in BE and TTFS-BE. (f) Rate capability of Li||NCM811 cells in BE and TTFS-BE. (g) Schematic illustration of commercial electrolyte comprised of BE with and without TTFS additive stored in air atmosphere for 12 h at a RH of 50%. (h) The corresponding first charge-discharge curves of Li ||NCM811 cells using the electrolytes in g.

To delve into the positive impact of TTFS on the cathode further, Li||NCM811 cells were disassembled after 100 cycles at room temperature, and an in-depth examination was conducted via XPS tests on the NCM811 cathode. The Si 2p energy spectrum derived from the XPS test distinctly illustrated the role of TTFS in the formation of the CEI, as depicted in **Figure 4**a and b, aligning with both prior experimental findings and theoretical insights. Notably, the silicon-rich CEI layer engendered by TTFS was found to enhance the high-temperature stability of the cathode.[51] Subsequent examination through transmission electron microscopy (TEM) tests unveiled the impact of TTFS on the CEI layer on the surface of the NCM811 cathode. As exhibited in Figure 4e and f, after 100 cycles at room temperature, the application of TTFS-BE resulted in the formation of a thinner and more uniform CEI layer, contrasting with the thicker and non-uniform CEI layer formed using BE. Furthermore, the crystal structure of the NCM811 cathode surface remained well-preserved throughout the cycling process, attributable to the incorporation of TTFS, as evidenced in Figure S8. The rationale behind this behavior can be inferred from the F 1s spectrum at the cathode surface, presented in Figure 4c and d, indicating that the heightened intensity of the C−F peaks correlates with the abundance of C−F bonds introduced by TTFS. In contrast, the elevated LiF content in BE arose from the decomposition of $LiPF_6$, a process effectively mitigated by TTFS. The stability of the CEI formed by TTFS was verified by determining the content of transition metals (Ni, Co and Mn) in the electrolyte using Inductively coupled plasma optical emission spectrometer (ICP-OES). Addition of TTFS effectively suppressed the dissolution of transition metals in the cathode of NCM811, thus inhibiting HF production and facilitating the formation of a robust CEI, as illustrated in Figure 4g and S9. X-ray diffraction (XRD)

results showed that the crystal structure (003 peak) of NCM811 remained well preserved even after 100 cycles at ambient temperature (Figure 4h and S10). A schematic detailing how TTFS protects the NCM811 cathode is presented in Figure 4i. The inclusion of TTFS not only mitigates the impact of $LiPF_6$ hydrolysis on the NCM811 cathode but also promotes the formation of an effective CEI.

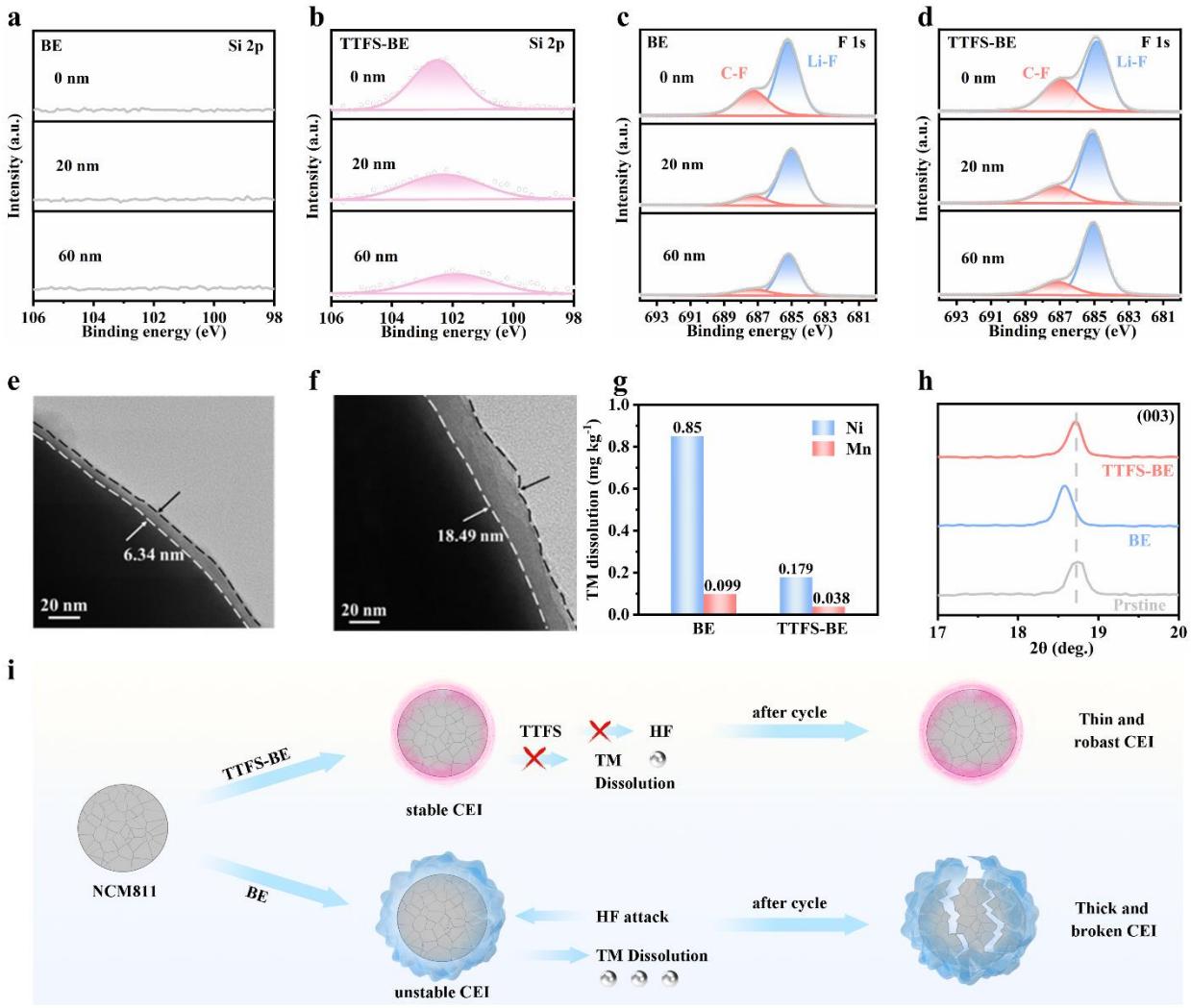

Figure 4. In depth (a) Si 2p and (c) F 1s XPS spectra of cycled NCM811 cathode in BE. (b) Si 2p and (d) F 1s XPS spectra of cycled NCM811 cathode in TTFS-BE. Ex situ TEM images of NCM811 cathodes in (e) BE with TTFS and (f) BE after 100 cycles. (g) ICP-OES of electrolytes storing fully charged NCM811 cathodes. (h) XRD patterns of NCM811 cathodes after 100 cycles. (i) Schematic illustration of the working mechanism of TTFS additive on the NCM811 cathode.

To investigate the effect of TTFS on Li metal anodes, Li||Li cells were assembled with TTFS-BE and BE. The Li||Li cell assembled with TTFS-BE demonstrated a stable long-cycle performance of up to 500 h, while the cell assembled with BE cycled stably for only 250 h, as illustrated in **Figure 5**a. The

utilization of TTFS-BE effectively stabilized the Li||Li cell, resulting in a notable improvement in cycling performance. This enhancement is evidenced by the observation that the introduction of TTFS more than doubled the cycling durability of Li||Li cells. Furthermore, in order to explore the impact of TTFS on the reversible performance of Li plating and stripping, Li||Cu cells were constructed using different electrolytes. The differences in CE of these electrolytes and their effects on the long-cycle performance of Li||Cu cells were evaluated. The Li||Cu cell underwent cycling at a constant capacity of 1 mA cm^{-2} at 1 mAh cm^{-2}, as depicted in Figure 5b. The experimental findings revealed a rapid decay in the CE of the cell assembled with BE after 55 cycles. This decay was attributed to the instability of the SEI on the electrode surface, resulting from parasitic reactions between the electrolyte and the electrodes, as well as the continuous hydrolysis of $LiPF_6$. Notably, the Li||Cu cells assembled with TTFS-BE exhibited significantly less decay over 90 cycles. This outcome demonstrates that the incorporation of TTFS effectively mitigated the damaging effects of $LiPF_6$ hydrolysis on the anode, by forming a chemically robust SEI to protect the anode from degradation.

In order to assess the impact of TTFS on the Li plating and stripping behavior, as well as the cycling performance of Li||NCM811 cells, different electrolytes were used to assemble the cells. The cells were cycled for 100 cycles at 1 C at room temperature, following which they were disassembled for scanning electron microscopy (SEM) analysis of the Li anode. Upon visual inspection of the SEM image presented in Figure 5c and S11, it was observed that there was significant formation of mossy dendrites on the surface of the Li anode when using the BE. These dendrites pose a risk of puncturing the diaphragm, potentially leading to battery short circuits and associated safety hazards. In contrast, the incorporation of TTFS resulted in a distinct change in the surface morphology of the Li anode, manifesting as a smooth and uniform surface without Li dendrite formation. This effect can be attributed to TTFS inhibiting the electrolyte decomposition and facilitating the formation of a robust SEI on the

electrode surface. Subsequent SEM analysis on the cross-section of the Li anode (Figure 5d) revealed that the Li deposition was thin and uniform following the addition of TTFS. Conversely, in the case of BE, the Li deposition appeared thicker and non-uniform due to the accumulation of electrolyte decomposition by-products on the Li surface, as well as the continuous growth of dendrites.

After 100 cycles at 1 C, a Li||NCM811 cell was disassembled to conduct in-depth XPS tests on the Li anode surface, aiming to investigate the mechanism of TTFS on Li plating and stripping (Figure 5e-h). The F 1s energy spectrum exhibited two peaks (Li−F and C−F), recognized as common components of the SEI. Notably, with the inclusion of TTFS, the surface C−F intensity in the SEI surpassed that of the BE. As the etching depth increased, the Li−F content gradually predominated. The foundation layer of LiF, known for its superior electronic insulation properties and mechanical strength in suppressing dendrite formation, was enhanced by TTFS.[52–56] On the other hand, the surface layer, abundant in C−F bonding, bestowed the SEI with a flexible outer layer capable of enduring the volume fluctuations of the Li anode throughout cycling, thereby hindering dendrite growth. In addition, analysis from Figure S12 reveals that the fluorine content in the SEI of TTFS-BE surpasses that of BE. The higher fluorine content signifies more involvement of fluoride in SEI formation, a factor known to improve SEI stability and enhance the battery cycle life. Thus, this organic-inorganic gradient fluorine-rich SEI conferred long-term stability to the Li anode during cycling. The heightened presence of LiF on the BE surface origins from the disintegration of $LiPF_6$, showcasing TTFS's inhibitory impact on $LiPF_6$ hydrolysis, a correlation also evident in the P 2p energy spectra. Li_xPF_y and $Li_xPO_yF_z$ were recognized as distinctive peaks resulting from $LiPF_6$ decomposition. Comparative analysis revealed reduced P 2p contents in SEIs formed by TTFS-BE, specifically in $Li_xPO_yF_z$, signifying TTFS's effective inhibition of $LiPF_6$ hydrolysis. Finally, we investigated the potential redox mechanism of TTFS. TTFS underwent a series of oxidation reactions on the cathode side, generating 1,1,1-trifluoropropane (TFP) and siloxane

products, which are considered to contribute to the formation of more stable CEI, as seen in Figure S13. On the anode side, TTFS was reduced and reacted with Li^+ to produce Li−F and C−F bond-containing products. These compounds were then involved in the formation of the SEI, leading to the formation of an organic-inorganic composite SEI. Particularly noteworthy is the role of TTFS in preventing the hydrolysis of $LiPF_6$ through the spontaneous trapping of H_2O and HF. This property of TTFS contributes significantly to the formation of stable SEI and CEI, highlighting its crucial function in the electrode interface reaction and its ability to enhance the stability of both SEI and CEI. These findings underscore the pivotal role played by TTFS in the enhancement of battery performance.

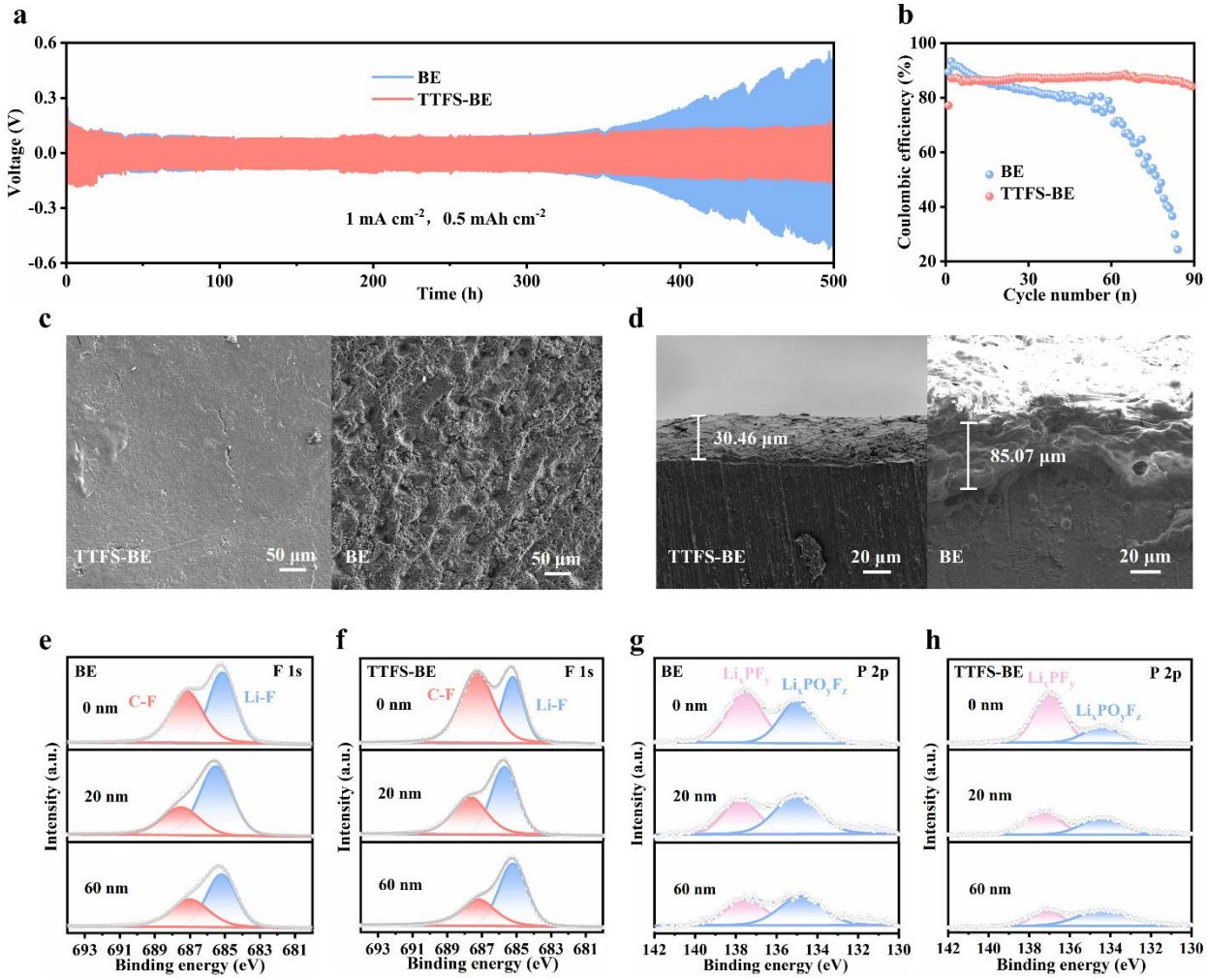

Figure 5. (a) Cycling performance of Li||Li cells using the BE and TTFS-BE with a current density of 1 mA cm^{-2} and a capacity of 0.5 mAh cm^{-2} (b) Cycling performance of Li||Cu cells using the BE and TTFS-BE with a current density of 1 mA cm^{-2} and a capacity of 1 mAh cm^{-2}. (c) surface and (d) cross-section SEM images of Li anode in BE and TTFS-BE after 100 cycles. In depth (e) F 1s and (g) P 2p

XPS spectra of cycled Li anode in BE. (g) F 1s and (h) P 2p XPS spectra of cycled Li anode in TTFS-BE.

Conclusions

In summary, we have demonstrated that stable cycling in LMBs can be achieved by incorporating a multifunctional sacrificial additive, TTFS, into common commercial electrolytes. The presence of strong Si−O bond in TTFS enables it to effectively capture trace H_2O in the electrolyte and inhibit the formation of HF to protect the high-nickel ternary cathodes and Li anodes. Moreover, TTFS plays a crucial role in mitigating the hydrolysis and solvent breakdown of $LiPF_6$ by altering the Li^+ solvation structure. Its distinctive chemical properties, characterized by a higher HOMO and lower LUMO, facilitate its preferential involvement in the formation of the SEI on both anodes and cathodes, thereby enhancing the long-term cycling stability of LMBs. As a result, the Li||NCM811 cell with TTFS additive achieves a capacity retention rate of 62.1% after 500 cycles at 1 C at 25℃ and 81.2% after 160 cycles at a high temperature of 60℃. This work points towards achieving durable electrolytes by multifunctional sacrificial additives in practical LMBs.

Supporting Information

Supporting Information is available from the author.

Conflict of Interest

The authors declare no conflict of interest.

Acknowledgements

We gratefully acknowledge the support from the National Natural Science Foundation of China (21805018; 52002039), the Natural Science Foundation of Sichuan Province (24NSFSC4536), the Scientific Research Startup Foundation of Chengdu University of Technology (10912-KYQD2023-

10240), and the Agency for Science, Technology and Research (MTC Programmatic Fund M23L9b0052 and Central Research Fund Award).

References

[1] Y. Xia, P. Zhou, X. Kong, J. Tian, W. Zhang, S. Yan, W. Hou, H.-Y. Zhou, H. Dong, X. Chen, P. Wang, Z. Xu, L. Wan, B. Wang, K. Liu, Designing an asymmetric ether-like lithium salt to enable fast-cycling high-energy lithium metal batteries, Nature Energy 8 (2023) 934–945. https://doi.org/10.1038/s41560-023-01282-z.

[2] Y. Meng, D. Zhou, R. Liu, Y. Tian, Y. Gao, Y. Wang, B. Sun, F. Kang, M. Armand, B. Li, G. Wang, D. Aurbach, Designing phosphazene-derivative electrolyte matrices to enable high-voltage lithium metal batteries for extreme working conditions, Nature Energy 8 (2023) 1023–1033. https://doi.org/10.1038/s41560-023-01339-z.

[3] W. Zhang, V. Koverga, S. Liu, J. Zhou, J. Wang, P. Bai, S. Tan, N.K. Dandu, Z. Wang, F. Chen, J. Xia, H. Wan, X. Zhang, H. Yang, B.L. Lucht, A.-M. Li, X.-Q. Yang, E. Hu, S.R. Raghavan, A.T. Ngo, C. Wang, Single-phase local-high-concentration solid polymer electrolytes for lithium-metal batteries, Nature Energy (2024). https://doi.org/10.1038/s41560-023-01443-0.

[4] H. Wan, Z. Wang, W. Zhang, X. He, C. Wang, Interface design for all-solid-state lithium batteries, Nature 623 (2023) 739–744. https://doi.org/10.1038/s41586-023-06653-w.

[5] C. Zhao, Z. Yan, B. Zhou, Y. Pan, A. Hu, M. He, J. Liu, J. Long, Identifying the Role of Lewis-base Sites for the Chemistry in Lithium-Oxygen Batteries, Angewandte Chemie International Edition 62 (2023) e202302746. https://doi.org/10.1002/anie.202302746.

[6] A.Y.S. Eng, C.B. Soni, Y. Lum, E. Khoo, Z. Yao, S.K. Vineeth, V. Kumar, J. Lu, C.S. Johnson, C. Wolverton, Z.W. Seh, Theory-guided experimental design in battery materials research, Science Advances 8 (2022) eabm2422. https://doi.org/10.1126/sciadv.abm2422.

[7] S. Zhang, X. Zhuang, X. Du, X. Zhang, J. Li, G. Xu, Z. Ren, Z. Cui, L. Huang, S. Wang, F. Sun, L. Qiao, S. Dong, G. Cui, A Novel Potassium Salt Regulated Solvation Chemistry Enabling Excellent Li-Anode Protection in Carbonate Electrolytes, Advanced Materials 35 (2023) 2301312. https://doi.org/10.1002/adma.202301312.

[8] Z. Wang, H. Zhang, J. Xu, A. Pan, F. Zhang, L. Wang, R. Han, J. Hu, M. Liu, X. Wu, Advanced Ultralow-Concentration Electrolyte for Wide-Temperature and High-Voltage Li-Metal Batteries, Advanced Functional Materials 32 (2022) 2112598. https://doi.org/10.1002/adfm.202112598.

[9] T. Liu, J. Wang, Y. Xu, Y. Zhang, Y. Wang, Dendrite-Free and Stable Lithium Metal Battery Achieved by a Model of Stepwise Lithium Deposition and Stripping, Nano-Micro Letters 13 (2021) 170. https://doi.org/10.1007/s40820-021-00687-3.

[10] Q. Peng, Z. Liu, L. Jiang, Q. Wang, Optimized Cycle and Safety Performance of Lithium–Metal Batteries with the Sustained-Release Effect of Nano $CaCO_3$, Advanced Energy Materials 12 (2022) 2104021. https://doi.org/10.1002/aenm.202104021.

[11] A. Hu, W. Chen, X. Du, Y. Hu, T. Lei, H. Wang, L. Xue, Y. Li, H. Sun, Y. Yan, J. Long, C. Shu, J. Zhu, B. Li, X. Wang, J. Xiong, An Artificial Hybrid Interphase For An Ultrahigh-Rate And Practical Lithium Metal Anode, Energy & Environmental Science 14 (2021) 4115–4124. https://doi.org/10.1039/D1EE00508A.

[12] W. Tang, T. Zhao, K. Wang, T. Yu, R. Lv, L. Li, F. Wu, R. Chen, Dendrite-Free Lithium Metal Batteries Enabled by Coordination Chemistry in Polymer-Ceramic Modified Separators, Advanced Functional Materials (2024) 2314045. https://doi.org/10.1002/adfm.202314045.
[13] S.-J. Yang, J.-K. Hu, F.-N. Jiang, H. Yuan, H.S. Park, J.-Q. Huang, Safer solid-state lithium metal batteries: Mechanisms and strategies, InfoMat 6 (2024) e12512. https://doi.org/10.1002/inf2.12512.
[14] Y.-T. Xu, S.-J. Dai, X.-F. Wang, X.-W. Wu, Y.-G. Guo, X.-X. Zeng, An ion-percolating electrolyte membrane for ultrahigh efficient and dendrite-free lithium metal batteries, InfoMat 5 (2023) e12498. https://doi.org/10.1002/inf2.12498.
[15] Y. Zhang, B. Wu, G. Mu, C. Ma, D. Mu, F. Wu, Recent progress and perspectives on silicon anode: Synthesis and prelithiation for LIBs energy storage, Journal of Energy Chemistry 64 (2022) 615–650. https://doi.org/10.1016/j.jechem.2021.04.013.
[16] B. Yang, Y. Pan, T. Li, A. Hu, K. Li, B. Li, L. Yang, J. Long, High-safety lithium metal pouch cells for extreme abuse conditions by implementing flame-retardant perfluorinated gel polymer electrolytes, Energy Storage Materials 65 (2024) 103124. https://doi.org/10.1016/j.ensm.2023.103124.
[17] C. Zhao, Y. Pan, R. Li, A. Hu, B. Zhou, M. He, J. Chen, Z. Yan, Y. Fan, N. Chen, M. Liu, J. Long, A safe anode-free lithium metal pouch cell enabled by integrating stable quasi-solid electrolytes with oxygen-free cathodes, Chemical Engineering Journal 463 (2023) 142386. https://doi.org/10.1016/j.cej.2023.142386.
[18] J. Xu, J. Zhang, T.P. Pollard, Q. Li, S. Tan, S. Hou, H. Wan, F. Chen, H. He, E. Hu, K. Xu, X.-Q. Yang, O. Borodin, C. Wang, Electrolyte design for Li-ion batteries under extreme operating conditions, Nature 614 (2023) 694–700. https://doi.org/10.1038/s41586-022-05627-8.
[19] J. Liu, X. Hu, S. Qi, Y. Ren, Y. Li, J. Ma, Research progress in failure mechanisms and electrolyte modification of high-voltage nickel-rich layered oxide-based lithium metal batteries, InfoMat 6 (2024) e12507. https://doi.org/10.1002/inf2.12507.
[20] F. Wu, A. Mullaliu, T. Diemant, D. Stepien, T.N. Parac-Vogt, J.-K. Kim, D. Bresser, G.-T. Kim, S. Passerini, Beneficial impact of lithium bis(oxalato)borate as electrolyte additive for high-voltage nickel-rich lithium-battery cathodes, InfoMat 5 (2023) e12462. https://doi.org/10.1002/inf2.12462.
[21] R. Zhang, S. Yang, H. Li, T. Zhai, H. Li, Air sensitivity of electrode materials in Li/Na ion batteries: Issues and strategies, InfoMat 4 (2022) e12305. https://doi.org/10.1002/inf2.12305.
[22] F. Li, J. Liu, J. He, Y. Hou, H. Wang, D. Wu, J. Huang, J. Ma, Additive-Assisted Hydrophobic Li+-Solvated Structure for Stabilizing Dual Electrode Electrolyte Interphases through Suppressing LiPF6 Hydrolysis, Angewandte Chemie International Edition 61 (2022) e202205091. https://doi.org/10.1002/anie.202205091.
[23] D. Zhang, M. Liu, J. Ma, K. Yang, Z. Chen, K. Li, C. Zhang, Y. Wei, M. Zhou, P. Wang, Y. He, W. Lv, Q.-H. Yang, F. Kang, Y.-B. He, Lithium hexamethyldisilazide as electrolyte additive for efficient cycling of high-voltage non-aqueous lithium metal batteries, Nature Communications 13 (2022) 6966. https://doi.org/10.1038/s41467-022-34717-4.
[24] K. Kim, H. Ma, S. Park, N.-S. Choi, Electrolyte-Additive-Driven Interfacial Engineering for High-Capacity Electrodes in Lithium-Ion Batteries: Promise and Challenges, ACS Energy Letters 5 (2020) 1537–1553. https://doi.org/10.1021/acsenergylett.0c00468.
[25] L. Li, D. Wang, G. Xu, Q. Zhou, J. Ma, J. Zhang, A. Du, Z. Cui, X. Zhou, G. Cui, Recent progress on electrolyte functional additives for protection of nickel-rich layered oxide cathode materials, Journal of Energy Chemistry 65 (2022) 280–292. https://doi.org/10.1016/j.jechem.2021.05.049.

[26] W. Xue, M. Huang, Y. Li, Y.G. Zhu, R. Gao, X. Xiao, W. Zhang, S. Li, G. Xu, Y. Yu, P. Li, J. Lopez, D. Yu, Y. Dong, W. Fan, Z. Shi, R. Xiong, C.-J. Sun, I. Hwang, W.-K. Lee, Y. Shao-Horn, J.A. Johnson, J. Li, Ultra-high-voltage Ni-rich layered cathodes in practical Li metal batteries enabled by a sulfonamide-based electrolyte, Nature Energy 6 (2021) 495–505. https://doi.org/10.1038/s41560-021-00792-y.

[27] J. Zhang, Q. Li, Y. Zeng, Z. Tang, D. Sun, D. Huang, Y. Tang, H. Wang, Weakly Solvating Cyclic Ether Electrolyte for High-Voltage Lithium Metal Batteries, ACS Energy Letters 8 (2023) 1752–1761. https://doi.org/10.1021/acsenergylett.3c00181.

[28] M. Sun, Y. Xie, C. Zhong, Y. Huang, H. Chen, H. Huang, P. Dai, S. Liu, W. Zheng, C. Liu, S. Liao, L. Huang, S. Sun, X. Wang, Bianionic coordination solvation structure electrolyte for high-voltage lithium metal batteries, Energy Storage Materials 65 (2024) 103166. https://doi.org/10.1016/j.ensm.2023.103166.

[29] A. Hu, F. Li, W. Chen, T. Lei, Y. Li, Y. Fan, M. He, F. Wang, M. Zhou, Y. Hu, Y. Yan, B. Chen, J. Zhu, J. Long, X. Wang, J. Xiong, Ion Transport Kinetics in Low-Temperature Lithium Metal Batteries, Advanced Energy Materials 12 (2022) 2202432. https://doi.org/10.1002/aenm.202202432.

[30] Q.-K. Zhang, X.-Q. Zhang, J. Wan, N. Yao, T.-L. Song, J. Xie, L.-P. Hou, M.-Y. Zhou, X. Chen, B.-Q. Li, R. Wen, H.-J. Peng, Q. Zhang, J.-Q. Huang, Homogeneous and mechanically stable solid–electrolyte interphase enabled by trioxane-modulated electrolytes for lithium metal batteries, Nature Energy 8 (2023) 725–735. https://doi.org/10.1038/s41560-023-01275-y.

[31] Q. Zhang, S. Liu, Z. Lin, K. Wang, M. Chen, K. Xu, W. Li, Highly safe and cyclable Li-metal batteries with vinylethylene carbonate electrolyte, Nano Energy 74 (2020) 104860. https://doi.org/10.1016/j.nanoen.2020.104860.

[32] Q.-K. Zhang, S.-Y. Sun, M.-Y. Zhou, L.-P. Hou, J.-L. Liang, S.-J. Yang, B.-Q. Li, X.-Q. Zhang, J.-Q. Huang, Reforming the Uniformity of Solid Electrolyte Interphase by Nanoscale Structure Regulation for Stable Lithium Metal Batteries, Angewandte Chemie International Edition 62 (2023) e202306889. https://doi.org/10.1002/anie.202306889.

[33] F. Wu, A. Mullaliu, T. Diemant, D. Stepien, T.N. Parac-Vogt, J.-K. Kim, D. Bresser, G.-T. Kim, S. Passerini, Beneficial impact of lithium bis(oxalato)borate as electrolyte additive for high-voltage nickel-rich lithium-battery cathodes, InfoMat 5 (2023) e12462. https://doi.org/10.1002/inf2.12462.

[34] J. Huang, H. Zhang, X. Yuan, Y. Sha, J. Li, T. Dong, Y. Song, S. Zhang, Regulating robust interphase using a functional ionic liquid additive with bi-electrode affinity to stabilize the high-voltage lithium-rich lithium metals batteries, Chemical Engineering Journal 464 (2023) 142578. https://doi.org/10.1016/j.cej.2023.142578.

[35] C. Liu, Z. Yuan, K. Chen, Y. Jiang, M. Yue, K. Dong, Y. Liu, Y. Guo, Y. Wang, MXene-BN-Introduced Artificial SEI to Inhibit Dendrite Growth of Lithium Metal Batteries, ACS Applied Materials & Interfaces 15 (2023) 56356–56364. https://doi.org/10.1021/acsami.3c09631.

[36] G. Wang, M. Zhu, Y. Zhang, C. Song, X. Zhu, Z. Huang, Y. Zhang, F. Yu, G. Xu, M. Wu, H.-K. Liu, S.-X. Dou, C. Wu, Double interface regulation: Toward highly stable lithium metal anode with high utilization, InfoMat 4 (2022) e12293. https://doi.org/10.1002/inf2.12293.

[37] B. Zhou, T. Li, A. Hu, B. Li, R. Li, C. Zhao, N. Chen, M. He, J. Liu, J. Long, Scalable fabrication of ultra-fine lithiophilic nanoparticles encapsulated in soft buffered hosts for long-life anode-free Li2S-based cells, Nanoscale 15 (2023) 15318–15327. https://doi.org/10.1039/D3NR03035K.

[38] Y. Li, A. Hu, X. Gan, M. He, J. Zhu, W. Chen, Y. Hu, T. Lei, F. Li, Y. Li, Y. Fan, F. Wang, M. Zhou, A. Wen, B. Li, Synergy of in-situ heterogeneous interphases tailored lithium deposition, Nano Research 16 (2023) 8304–8312. https://doi.org/10.1007/s12274-022-5004-0.
[39] R. Li, Y. Fan, C. Zhao, A. Hu, B. Zhou, M. He, J. Chen, Z. Yan, Y. Pan, J. Long, Air-Stable Protective Layers for Lithium Anode Achieving Safe Lithium Metal Batteries, Small Methods 7 (2023) 2201177. https://doi.org/10.1002/smtd.202201177.
[40] B. Jiang, H. Li, B. Luo, L. Liu, L. Chu, Q. Zhang, M. Li, Vinyltrimethylsilane as a novel electrolyte additive for improving interfacial stability of Li-rich cathode working in high voltage, Chinese Chemical Letters 35 (2024) 108649. https://doi.org/10.1016/j.cclet.2023.108649.
[41] Y. Wang, N. Dong, B. Liu, G. Tian, S. Qi, D. Wu, Self-adaptive Gel Poly(imide-siloxane) Binder Ensuring Stable Cathode-Electrolyte Interface for Achieving High-Performance NCM811 Cathode in Lithium-ion Batteries, Energy Storage Materials 56 (2023) 621–630. https://doi.org/10.1016/j.ensm.2023.02.002.
[42] S. Zhang, M. He, C.-C. Su, Z. Zhang, Advanced electrolyte/additive for lithium-ion batteries with silicon anode, Current Opinion in Chemical Engineering 13 (2016) 24–35. https://doi.org/10.1016/j.coche.2016.08.003.
[43] H. Sun, J. Liu, J. He, H. Wang, G. Jiang, S. Qi, J. Ma, Stabilizing the cycling stability of rechargeable lithium metal batteries with tris(hexafluoroisopropyl)phosphate additive, Science Bulletin 67 (2022) 725–732. https://doi.org/10.1016/j.scib.2022.01.012.
[44] L. Yu, S. Chen, H. Lee, L. Zhang, M.H. Engelhard, Q. Li, S. Jiao, J. Liu, W. Xu, J.-G. Zhang, A Localized High-Concentration Electrolyte with Optimized Solvents and Lithium Difluoro(oxalate)borate Additive for Stable Lithium Metal Batteries, ACS Energy Letters 3 (2018) 2059–2067. https://doi.org/10.1021/acsenergylett.8b00935.
[45] H.J. Kim, N. Umirov, J.-S. Park, J.-H. Lim, J. Zhu, S.-S. Kim, S.-T. Myung, Lithium dendritic growth inhibitor enabling high capacity, dendrite-free, and high current operation for rechargeable lithium batteries, Energy Storage Materials 46 (2022) 76–89. https://doi.org/10.1016/j.ensm.2022.01.002.
[46] H. Li, Z. Wen, D. Wu, W. Ji, Z. He, F. Wang, Y. Yang, P. Zhang, J. Zhao, Achieving a Stable Solid Electrolyte Interphase and Enhanced Thermal Stability by a Dual-Functional Electrolyte Additive toward a High-Loading LiNi0.8Mn0.1Co0.1O2 /Lithium Pouch Battery, ACS Applied Materials & Interfaces 13 (2021) 57142–57152. https://doi.org/10.1021/acsami.1c17209.
[47] S.H. Lee, J.-Y. Hwang, S.-J. Park, G.-T. Park, Y.-K. Sun, Adiponitrile (C6H8N2): A New Bi-Functional Additive for High-Performance Li-Metal Batteries, Advanced Functional Materials 29 (2019) 1902496. https://doi.org/10.1002/adfm.201902496.
[48] Z. Ren, H. Qiu, C. Fan, S. Zhang, Q. Zhang, Y. Ma, L. Qiao, S. Wang, G. Xu, Z. Cui, G. Cui, Delicately Designed Cyano-Siloxane as Multifunctional Additive Enabling High Voltage LiNi 0.9 Co 0.05 Mn 0.05 O 2 /Graphite Full Cell with Long Cycle Life at 50 °C, Advanced Functional Materials (2023) 2302411. https://doi.org/10.1002/adfm.202302411.
[49] Y. Chen, Q. He, Y. Mo, W. Zhou, Y. Zhao, N. Piao, C. Liu, P. Xiao, H. Liu, B. Li, S. Chen, L. Wang, X. He, L. Xing, J. Liu, Engineering an Insoluble Cathode Electrolyte Interphase Enabling High Performance NCM811//Graphite Pouch Cell at 60 °C, Advanced Energy Materials 12 (2022) 2201631. https://doi.org/10.1002/aenm.202201631.
[50] F. Li, J. He, J. Liu, M. Wu, Y. Hou, H. Wang, S. Qi, Q. Liu, J. Hu, J. Ma, Gradient Solid Electrolyte Interphase and Lithium-Ion Solvation Regulated by Bisfluoroacetamide for Stable Lithium Metal

Batteries, Angewandte Chemie International Edition 60 (2021) 6600–6608. https://doi.org/10.1002/anie.202013993.

[51] H. Wang, S. Chen, Y. Li, Y. Liu, Q. Jing, X. Liu, Z. Liu, X. Zhang, Organosilicon-Based Functional Electrolytes for High-Performance Lithium Batteries, Advanced Energy Materials 11 (2021) 2101057. https://doi.org/10.1002/aenm.202101057.

[52] Q.-K. Zhang, S.-Y. Sun, M.-Y. Zhou, L.-P. Hou, J.-L. Liang, S.-J. Yang, B.-Q. Li, X.-Q. Zhang, J.-Q. Huang, Reforming the Uniformity of Solid Electrolyte Interphase by Nanoscale Structure Regulation for Stable Lithium Metal Batteries, Angewandte Chemie International Edition 62 (2023) e202306889. https://doi.org/10.1002/anie.202306889.

[53] J.-L. Liang, S.-Y. Sun, N. Yao, Z. Zheng, Q.-K. Zhang, B.-Q. Li, X.-Q. Zhang, J.-Q. Huang, Regulating the electrolyte solvation structure by weakening the solvating power of solvents for stable lithium metal batteries, Science China Chemistry 66 (2023) 3620–3627. https://doi.org/10.1007/s11426-023-1730-x.

[54] S. Huang, Y.-P. Huang, Y. Xia, J. Ding, C. Peng, L. Wang, J. Luo, X.-X. Zhang, J. Zheng, Y.Q. Gao, J. Chen, High Li^+ coordinated solvation sheaths enable high-quality Li metal anode, InfoMat 5 (2023) e12411. https://doi.org/10.1002/inf2.12411.

[55] Y. Li, E. Mao, Z. Min, Z. Cai, Z. Chen, L. Fu, X. Duan, L. Wang, C. Zhang, Z. Lu, W. Liu, Z.W. Seh, Y. Sun, Hybrid Polymer-Alloy-Fluoride Interphase Enabling Fast Ion Transport Kinetics for Low-Temperature Lithium Metal Batteries, ACS Nano 17 (2023) 19459–19469. https://doi.org/10.1021/acsnano.3c08576.

[56] G. Li, X. Duan, X. Liu, R. Zhan, X. Wang, J. Du, Z. Chen, Y. Li, Z. Cai, Y. Shen, Y. Sun, Locking Active Li Metal through Localized Redistribution of Fluoride Enabling Stable Li-Metal Batteries, Advanced Materials 35 (2023) 2207310. https://doi.org/10.1002/adma.202207310.